Journal of Environmental Chemical Engineering 5 (2017) 1166–1173

Contents lists available at ScienceDirect

Journal of Environmental Chemical Engineering

journal homepage: www.elsevier.com/locate/jece

The effect of common groundwater anions on the aqueous corrosion of zero-valent iron nanoparticles and associated removal of aqueous copper and zinc

H. Pullin[a,*], R.A. Crane[b], D.J. Morgan[c], T.B. Scott[a]

[a] Interface Analysis Centre, School of Physics, Bristol University, BS8 1TL, UK
[b] Geoenvironmetal Research Centre, School of Engineering, Cardiff University, CF24 3AA, UK
[c] Cardiff Catalysis Institute, School of Chemistry, Cardiff University, CF10 3AT, UK

ARTICLE INFO

Article history:
Received 19 September 2016
Received in revised form 23 January 2017
Accepted 24 January 2017
Available online 31 January 2017

Keywords:
Iron nanoparticles
Anionic effects on corrosion
Groundwater
Cu and Zn sorption behaviour
Phase transition pathways

ABSTRACT

This work has investigated the influence of common groundwater anions (Cl^-, NO_3^-, SO_4^{2-} and HCO_3^-) on the corrosion behaviour and associated removal of copper (Cu) and zinc (Zn) ions onto nanoscale zero-valent iron particles (nZVI). After 16 week exposure to solutions containing each anion at 10 mM concentrations, nZVI was observed to corrode into different iron (hydr)oxide phases (determined using XRD), depending upon the anion present: HNO_3^- produced goethite particles; NO_3^- produced predominantly magnetite/maghemite particles; both SO_4^{2-} and Cl^- produced a mixture of phases, including magnetite/maghemite, lepidocrocite and goethite. For solutions containing the different anions and 0.3 mM concentrations of Cu or Zn, near-total metal removal onto nZVI was recorded in the initial stages of the reaction (e.g. <24 h) for all systems tested. However, when Cl^- and SO_4^{2-} were also present significant subsequent desorption was recorded and attributed to the influence of anionic pitting corrosion. In contrast, no Cu or Zn desorption was recorded for batch systems containing NO_3^-, which was attributed to the enmeshment of Cu or Zn in a mixed-valent iron oxide shell. Results herein therefore demonstrate that NO_3^- could be utilised alongside nZVI to improve its long-term performance for in situ water treatment applications.

1. Introduction

Aqueous contaminant transformation and/or removal by nanoscale zero-valent iron particles (nZVI) is dependent upon the aqueous corrosion pathway and fate of the particles. The corrosion process is dependent upon a range of different factors including time, dissolved oxygen (DO) concentration, organic matter concentration, pH and the concentration of common groundwater cations and anions [1,2].

To date, the majority of empirical studies have investigated contaminant removal onto nZVI using "chemically simple" solutions, i.e. deionised water plus the contaminant of interest, which is far removed from the geochemical complexity of natural waters. The influence of common groundwater anions on the removal and retention of aqueous contaminants by nZVI is therefore of great interest. The major groundwater anions are chloride (Cl^-), bicarbonate (HCO_3^-) and sulphate (SO_4^{2-}), and are typically present at concentrations within the range of 1.0–1000 mg L^{-1}. Nitrate (NO_3^-) is less common and typically present at concentrations between 0.01–10 mg L^{-1}. NO_3^- contamination is a growing concern in the UK and many other countries, however, and as such concentrations are recorded to be rising at an average of 0.34 mg NO_3^- L per year [3].

Both Cl^- [2,4,5] and SO_4^{2-} [2,5] increase iron corrosion rates by destabilising any passivating films which may form. In contrast NO_3^- inhibits corrosion [2,5–7], and also acts to nullify the corrosion-promoting effect of Cl^- [8]. However, there have been limited studies investigating how such anions influence the corrosion pathway of nZVI. Reinsch et al. [9] exposed hydrogen-reduced nZVI to 10 mM solutions of Cl^-, HCO_3^-, NO_3^- and SO_4^{2-}. The passivation of nZVI was recorded in increasing order as HCO_3^-, SO_4^{2-}, Cl^- and NO_3^-. NO_3^- passivation was reported to be very influential; Fe^0 was still detected after 6 months aqueous exposure. Moreover Kanel et al. [10] recorded HCO_3^-, NO_3^- and SO_4^{2-} as not effecting As^{5+} uptake until anionic concentrations reached 10 mM. Furthermore Lim and Zhu [11] recorded NO_3^- as able to limit the

* Corresponding author at: IAC, HH Wills Physics Laboratory, Tyndall Avenue, Bristol, BS8 1TL, UK.
E-mail address: phxhp@bristol.ac.uk (H. Pullin).

http://dx.doi.org/10.1016/j.jece.2017.01.038

breakdown of TCE by bimetallic Fe-Pd nanoparticles at concentrations as low as 2 mM, whereas HCO_3^- exerted only a minor inhibitory influence. SO_4^{2-} did not exhibit a significant influence.

The corrosion experiments outlined above were performed using hydrogen reduced nZVI, which has been shown to be markedly less reactive than borohydride reduced particles [12]. Moreover the experimental time periods of these studies may not be of sufficient duration to ascertain final corrosion states of nZVI when exposed to common groundwater anions. In this work, we aimed to bridge these gaps in our understanding by investigating the removal efficacy of Cu and Zn ions (two very common groundwater contaminants) onto borohydride reduced nZVI in solutions also containing major groundwater anions (namely: HCO_3^-, Cl^-, SO_4^{2-} and NO_3^-).

2. Materials and methods

2.1. Chemicals

All chemicals (iron sulphate ($FeSO_4{\cdot}7H_2O$), nitric acid (HNO_3), sodium borohydride ($NaBH_4$), sodium hydroxide (NaOH), sodium bicarbonate ($NaHCO_3$), sodium chloride (NaCl), sodium nitrate ($NaNO_3$), sodium sulphate (Na_2SO_4), copper acetate ($Cu(CH_3COO)_2$), zinc acetate ($Zn(O_2CCH_3)_2$) and solvents (ethanol, acetone)) used in this study were of analytical grade.

2.2. nZVI synthesis

Pure nZVI was synthesised via the borohydride-reduction of ferrous iron [13]. First 7.6 g of $Fe_2(SO_4)_3{\cdot}6H_2O$ was dissolved in 200 mL of Milli-Q water (resistivity > 18.2 MΩ) that had been purged with oxygen free nitrogen gas for 10 min. The solution pH was then slowly adjusted to 6.8 by adding 4 M NaOH dropwise to prevent the formation of hydroxocarbonyl complexes. To this, 3.0 g of $NaBH_4$ was added (~0.2 g per min). The resultant solid material was cleaned through centrifugation and sequential rinsing in 50 mL of Milli-Q water, acetone and then ethanol. The nanoparticles were dried under low vacuum in a vacuum desiccator ($\sim 10^{-2}$ mbar), and then stored in an argon filled (BOC, 99.998%) MBraun glovebox until required.

2.3. Experimental procedure

To assess changes to nZVI structure, Schott-Duran jars (2 L) were filled with 1.6 L of a 10 mM sodium-anion solution. The bicarbonate solution was synthesised from sodium bicarbonate ($NaHCO_3$), the chloride solution from sodium chloride (NaCl), the nitrate solution from sodium nitrate ($NaNO_3$) and the sulphate solution from sodium sulphate (Na_2SO_4). From each batch 100 mL of solution was removed, to which 1.6 g of nZVI was added. This was sonicated for 5 min in a VWR USC100T ultrasonic cleaner to disperse the nanomaterial, and then returned to the parent jar. From these, 200 mL aliquots of nZVI-liquid suspensions were removed after 2 h, 1 d, 3 d, 1 w, 2 w, 4 w, 8 w, and 16 w.

Batch tests were performed with 400 mL solutions of Cl^-, NO_3^- and SO_4^{2-} anions at 0.1, 1.0 and 10.0 mM, with 0.3 mM (~20 mg L^{-1}) of a metal solution and 0.5 g L^{-1} nZVI. The influence of HCO_3^- on Cu and Zn uptake onto nZVI was not investigated due to the formation of insoluble Cu or Zn carbonate precipitates. The experimental matrix and starting pH and ORP (oxidation reduction potential) values are shown in Table 1. All batch tests were performed using Pyrex beakers. All batches were sonicated for 5 min after nZVI addition, and then covered loosely with Sarogold plastic film to allow gas exchange but to prevent evaporation/cross contamination. From these, 10 mL aliquots of nZVI suspensions were taken at 0 h, 1 h, 2 h, 1 d, 3 d, 1 w, 2 w and 4 w. Geochemical parameters (pH, ORP and DO) were measured concurrently using a Hach Multimeter (model HQ40d).

To ensure a homogenous sample was taken, all sample containers were gently agitated prior to sampling. The extracted nZVI suspensions were separated into solid and liquid phases via 10 min of centrifugation at 6500 rpm using an Eppendorf 5810 centrifuge (nZVI corrosion experiments) or for one minute using a Hamilton Bell Vanguard V6500 desktop centrifuge (Cu and Zn uptake experiments). The liquid supernatant was then syringe filtered through a 0.22 μm cellulose filter, and then acidified using 1% v/v nitric acid to prevent metal precipitation or adsorption to the sample vessel. The solid material was washed by the same cleaning method described in Section 2.2, and then stored under ultra-pure ethanol until required for further analysis (<24 h).

2.4. Sample analysis methods

A Phillips Xpert Pro diffractometer with a Cu Kα radiation source (λ = 1.5406 Å) was used for X-ray diffraction (XRD) analysis (generator voltage of 40 keV; tube current of 30 mA). XRD plots were acquired between 10 and 70 °2θ with a step size of 0.02 °2θ and a 2 s dwell time. Plots were compared to the following Joint Committee on Powder Diffraction Standards (JCPDS) cards: goethite 81-0463, lepidocrocite 74-1877, maghemite 39-1346 and magnetite 86-1362. Miller indices for the identified peaks are shown in Table S1 (Supplementary material). A Kratos AXIS ULTRA-DLD spectrometer employing a monochromatic X-ray source (Al K_α 1486.6 eV) was used for X-ray photoelectron spectroscopy (XPS) analysis. Survey scans were acquired using a pass energy of 160 eV and a 1 eV step, whilst high resolution spectra were acquired using a 40 eV pass energy and a 0.1 eV step. Data analysis was performed using CasaXPS software after subtraction of a Shirley background, and fitted following the method of Grosvenor et al. [14]. All spectra were calibrated to the C1s line taken to be 285 eV for adventitious carbon. In preparation for BET specific surface area (SSA) analysis, samples were degassed under vacuum ($\sim 10^{-2}$ mbar) for a 24 h period at a temperature of 75 °C. A known mass of this materials was then measured using a

Table 1
Experimental matrix and starting pH and ORP of solutions.

Concentration (mM)	Metal	Cl^-		NO_3^-		SO_4^{2-}		Controls	
		pH	ORP (mV)	pH	ORP (mV)	pH	ORP (mV)	pH	ORP (mV)
0	Cu							5.3	149
	Zn							6.3	140
0.1	Cu	5.0	238	5.4	278	5.4	159		
	Zn	5.6	120	5.4	74	6.3	107		
1.0	Cu	5.2	243	5.7	262	5.4	122		
	Zn	5.8	111	5.4	90	6.1	89		
10.0	Cu	5.3	150	5.9	237	5.6	46		
	Zn	6.1	41	5.6	99	5.9	46		

Quantachrome NOVA 1200 surface area analyser, with N_2 as the adsorbent and following a 7 point BET method. Transmission electron microscopy (TEM) images of nZVI mounted on 200 mesh holey carbon coated Cu grids were obtained with a JEOL JEM 1200 EX Mk 2 TEM operating at 120 keV. Inductively coupled optical emission spectrometry (ICP-OES) was used to determine the aqueous concentrations of Cu, Zn and iron (Fe). The instrument used was an Agilent 710 ICP-OES. Blanks and standards were prepared in 1% nitric acid.

3. Results

3.1. Preliminary characterisation of the nZVI

Characterisation of the as-formed nZVI revealed features that are commonly associated with borohydride-reduced nZVI [15]. Analysis by XPS and XRD indicated that the core of nZVI was poorly crystalline α-Fe (characteristic peak at 44.9°2θ) with a shell of mixed valent iron oxides/oxyhydroxides (Fig. 1). TEM analysis (Fig. 2) determined that the particles were roughly spherical, with a typical size range of 40–100 nm and no clear grain structure identified. BET analysis determined that the surface area of nZVI was 11.5 $m^2 g^{-1}$.

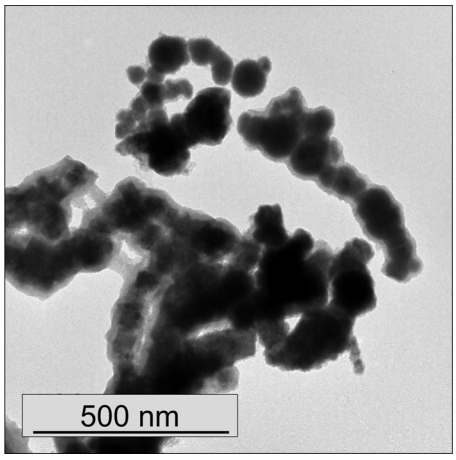

Fig. 2. TEM image acquired for the as-formed nZVI.

3.2. X-ray diffraction results from nZVI corrosion experiments

X-ray diffraction (XRD) plots for nZVI removed from the experimental solutions after 16 w are presented in Fig. 3. Previously published XRD data of nZVI removed from a solution without anions, but performed with the same experimental methodology, is also presented (hereafter, termed as the control) [16]. Time resolved XRD plots are presented in Figs. S1–S3 (Supplementary material). Crystal structure changes, as well as the relevant equations have been previously documented in Cornell and Schwertmann [17]. Crystal structural information for the identified minerals are shown in Table S2 (Supplementary material).

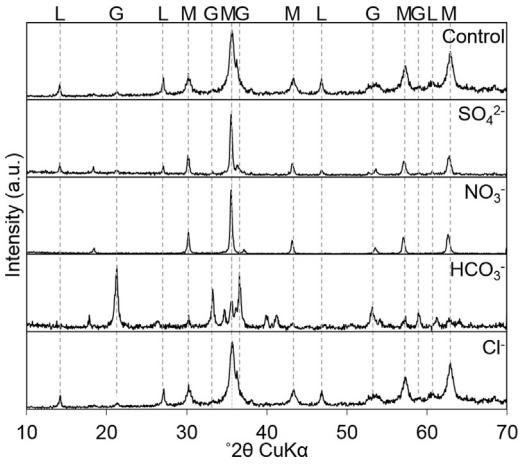

Fig. 3. X-ray diffraction plots with identified peaks for the range 10–70°2θ acquired for nZVI extracted from experimental solutions containing 10 mM Cl^-, HCO_3^-, NO_3^-, SO_4^{2-} and control (anion-free) after 16 w (ascending).
Key: G – α-FeOOH, L – γ-FeOOH and M – Fe_3O_4/γ-Fe_2O_3.

3.2.1. Influence of Cl^- on nZVI corrosion

The 10 mM Cl^- solution (Fig. S1, Supplementary material) was recorded to corrode the nZVI more rapidly than the control solution (solution of deionised water only), with the emergence of magnetite/maghemite (Fe_3O_4/γ-Fe_2O_3) after only 2 h (Fig. S3, Supplementary material). Due to the similar spinel crystal structure of Fe_3O_4 and γ-Fe_2O_3, their differentiation by XRD was not possible [9,18]. Lepidocrocite (γ-FeOOH), was identified after 1 w, and after 2 w, a small akaganéite (β-FeOOH) peak was observed. The latter iron requires chloride to form (alternative formula $Fe^{3+}O(OH,Cl)$) and proved to be transient, not appearing in any other scans. Zero-valent iron (44.9°2θ) was detected for up to 2 w, compared to 4 w for the control system. Only minor changes were observed between the 4 w material and the final 16 w material (Fe_3O_4/γ-Fe_2O_3 and γ-FeOOH were the main phases), although a single α-FeOOH peak at 21.3°2θ was also identified (Fig. 3).

3.2.2. Influence of HCO_3^- on nZVI corrosion

After an initial emergence of Fe_3O_4/γ-Fe_2O_3 after 2 h (Fig. S2, Supplementary material), the predominant phase identified was goethite (α-FeOOH), which was detected as a minor contribution after 1 d in conjunction with Fe_3O_4/γ-Fe_2O_3. No iron carbonate

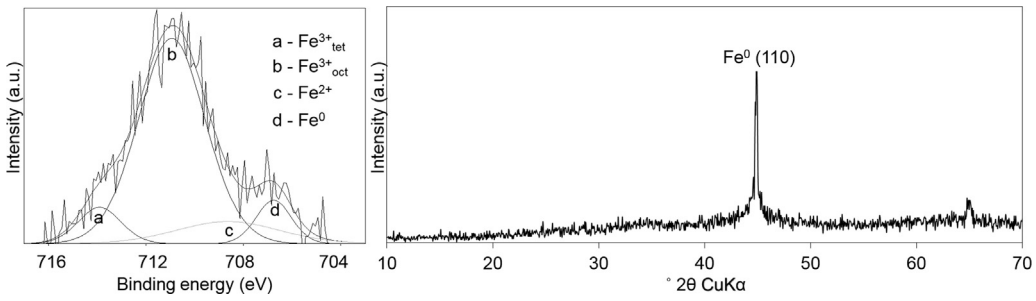

Fig. 1. Fitted X-ray photoelectron plot with fitted photoelectron peaks (left) and X-ray diffraction plot with identified peaks(for the range 10–70°2θ) (right) acquired for the as-formed nZVI.

phases (e.g. siderite) were identified. The Fe^0 peak (44.9°2θ) was not detected after 3 d. Similar to the aforementioned Cl^- bearing batch system, little difference was recorded between the 4 and 8 w XRD profiles (Fig. 3), with α-FeOOH the main phase identified, along with Fe_3O_4/γ-Fe_2O_3.

3.2.3. Influence of NO_3^- on nZVI corrosion

When exposed to a 10 mM NO_3^- solution (Fig. S2, Supplementary material) the nZVI was recorded to corrode more rapidly than the control (Fig. S3, Supplementary material), with the emergence of multiple Fe_3O_4/γ-Fe_2O_3 peaks after only 2 h and no identifiable Fe^0 peaks after only 1 d. Magnetite/maghemite remained the dominant phase throughout the experiment. No new peaks emerged after 3 d, and no significant changes were observed after 1 w. At 16 w, Fe_3O_4/γ-Fe_2O_3 was the sole phase(s) identified (Fig. 3).

3.2.4. Influence of SO_4^{2-} on nZVI corrosion

The corrosion pathway of nZVI in a 10 mM SO_4^{2-} solution (pH 5.7) (Fig. S2, Supplementary material) was recorded as broadly similar to when exposed to the 10 mM Cl^- solution (Fig. S1, Supplementary material). The final 16 w scans were relatively similar, with three differing phases identified: Fe_3O_4/γ-Fe_2O_3, γ-FeOOH and α-FeOOH. Fe_3O_4/γ-Fe_2O_3 was the first emergent phase (2 h), which was followed by γ-FeOOH (2 w) and subsequently α-FeOOH (8 w), although little difference was observed between the XRD data for 4 w and 16 w exposure times.

3.3. Aqueous Cu and Zn uptake onto nZVI experiments

3.3.1. Changes in ORP, pH and DO

For all batch systems, the addition of nZVI resulted in a rapid shift to chemically reducing conditions and an increase in pH. This was attributed to the rapid oxidation of nZVI, consuming DO and H^+ and increasing the ORP of the solution (Figs. S4 and S5, Supplementary material). All NO_3^- solutions recorded a greater pH shift than the control, but the opposite was recorded for the SO_4^{2-} and Cl^- bearing solutions. Of note, the pH of the Cl^- and SO_4^{2-} reverted to pre-treatment levels far sooner than the control or the NO_3^- solution, most pertinently when Zn was also present (<24 h). Furthermore, the pH levels continued to fall below the starting levels, indicating that in addition to a slowing of the nZVI corrosion rates, further reactions were also occurring. For 0.1 and 1.0 mM NO_3^- solutions treated with nZVI, regardless of metal contaminant, low ORP and DO (<3 mg L^{-1}) levels were maintained for the first 24–72 h of the experiment, followed by a gradual reversion to ambient conditions after this time. However, in the 10 mM solutions, ORP and DO levels did not reach the same levels as the lower molar solutions, and the reversion to ambient levels began at a much earlier time (~4 h or less). Furthermore, a different geochemical response was observed in the Cl^- and SO_4^{2-} solutions treated with nZVI, depending on whether Cu or Zn were present; DO in the Zn solutions began to return to ambient conditions much sooner (~4 h), compared to the Cu solutions (~24 h).

3.3.2. Removal of Cu and Zn by nZVI

The copper uptake mechanism by nano-Fe^0 has been reported to be via cementation [19], and therefore a source of electrons must be present (Eqs. (1)–(2)):

$$Cu^{2+}{}_{(aq)} + Fe^0{}_{(s)} \rightarrow Fe^{2+}{}_{(s)} + Cu^0{}_{(s)} \quad (1)$$

$$_{(aq)} + 2Fe^{2+}{}_{(s)} \rightarrow 2Fe^{3+}{}_{(s)} + Cu^0{}_{(s)}$$

Zinc is removed from solution by surface adsorption and complexation/precipitation, which may include electrostatic interactions and specific surface bonding, with no net electron transfer [19]. The changes in dissolved metal concentrations from the batch systems containing 0.1 and 1.0 mM of Cl^-, NO_3^- and SO_4^{2-} are summarised in Table 2. The changes in solution metal concentrations from the batch systems containing 10 mM of Cl^-, NO_3^- and SO_4^{2-} are summarised in Table 2 and shown in Fig. 4.

Considering the extremely low minimum metal concentrations reported in Table 2, it was concluded that solutions containing anions at concentrations up to 10.0 mM had little influence on the initial removal of both Cu and Zn from solution by nZVI as they were recorded at near-zero concentrations after ~1 h. However,

Table 2
Maximum removal and subsequent release of Cu and Zn (0.3 mM) by nZVI with the influence of Cl^-, SO_4^{2-} and NO_3^-.

Anion	Contaminant	Anion conc. (mM)	Minimum metal concentrations (mg L^{-1})	Remobilisation time (h)	Metal concentrations at 672 h (mg L^{-1})
Cl^-	Cu	0.1	ND	>24	6.473
		1.0	0.002	>24	6.849
		10.0	0.032	>24	8.389
	Zn	0.1	0.028	>1	1.148
		1.0	0.060	>1	1.410
		10.0	0.107	>1	11.231
SO_4^{2-}	Cu	0.1	ND	>24	6.756
		1.0	ND	>24	6.649
		10.0	ND	>48	8.361
	Zn	0.1	0.003	>2	1.052
		1.0	0.030	>2	1.182
		10.0	0.060	>1	13.303
NO_3^-	Cu	0.1	0.006	>336	0.124
		1.0	0.002	>336	0.199
		10.0	ND	>336	0.025
	Zn	0.1	0.068	>336	0.089
		1.0	ND	>168	0.003
		10.0	ND	>336	0.037
Control (anion-free)	Cu	N/A	ND	>24	6.799
	Zn	N/A	ND	>2	1.679
Blank (anion-nZVI free)	Cu	N/A	19.823		19.963
	Zn	N/A	19.734		19.894

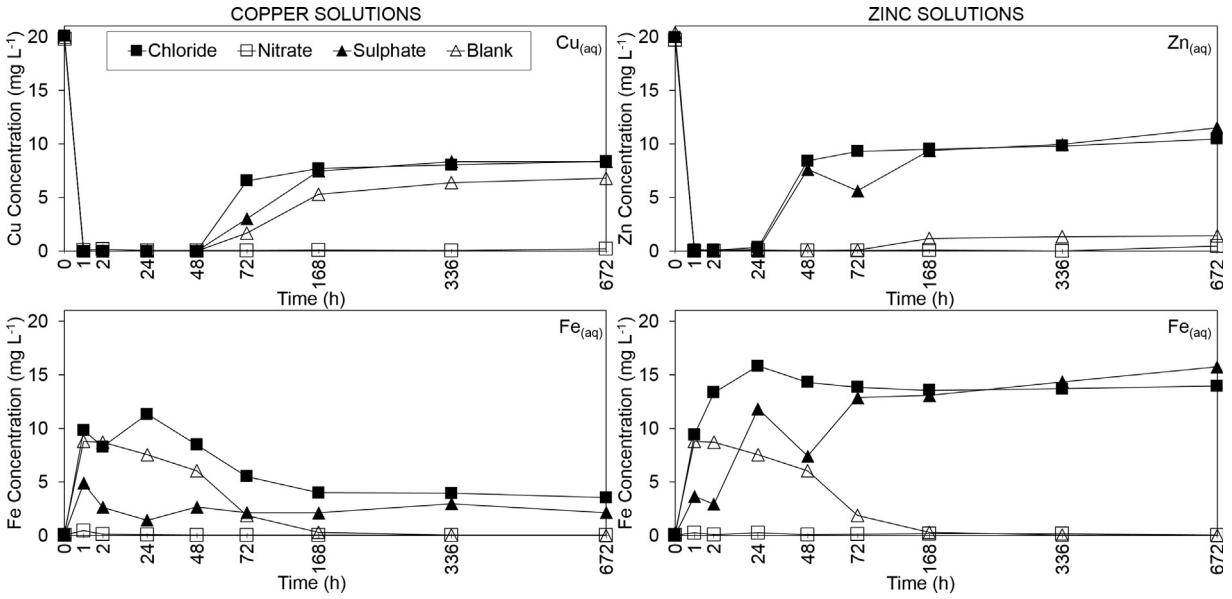

Fig. 4. Changes in aqueous metal (top) and iron (bottom) concentration (mg L^{-1}) in solutions containing copper (left) and zinc (right) and 10 mM anions when treated with nZVI, as a function of experimental time (672 h).
Note, different vertical scales. Note, instrument SD values were below 0.01 mg L^{-1}.
Key: Square – Chloride, Circle – Sulphate, Triangle – Nitrate and Cross – Blank.

when considering metal concentrations at the termination of the experiment in Table 2, it was concluded that differing anionic concentrations exerted a considerable influence on the remobilisation of contaminants into solutions.

For solutions containing Cl^- and SO_4^{2-} at concentrations <1.0 mM, similar aqueous Cu and Zn concentrations to the control were recorded at the termination of the experiment (Cu ~ 6.6 mg L^{-1}, Zn ~ 1.5 mg L^{-1}). However, for solutions containing such anions at 10 mM concentrations (Fig. 4), significant Cu and Zn remobilisation occurred, concurrent with higher concentrations of aqueous Fe. Furthermore, Fe concentrations continued to be elevated until the termination of the experiment, whereas, at lower anionic concentrations, aqueous Fe concentrations were at their highest levels generally for only ~1 h reaction time. This was followed by a reversion to extremely low concentrations after ~2 w (attributed to the oxidation of Fe^{2+} to the less soluble Fe^{3+}). Considering remobilisation times in Table 2, for solutions containing Cl^- and SO_4^-, Cu and Zn remobilisation occurred at different times, regardless of anionic concentrations, with Zn generally remobilising before Cu. In contrast, for all solutions containing NO_3^-, no Cu or Zn remobilisation was recorded, with the concentration of such metals recorded at the end of the experiment (16 w) as near-zero for all solutions regardless of anionic concentration.

3.3.3. Analysis of nZVI aqueous corrosion behaviour

X-ray diffraction plots of the nZVI extracted after 4 w reaction time from the zinc and copper bearing solutions containing 10 mM Cl^-, NO_3^- and SO_4^{2-} are presented in Fig. S6, Supplementary material; and plots from the 10 mM solutions are presented in Fig. 5. Magnetite/maghemite and γ-FeOOH were identified in the final XRD scans of nanomaterial exposed to the control solution (deionised water only), as well as the 10 mM Cl^- and SO_4^{2-} solutions, whereas a combination of Fe_3O_4/γ-Fe_2O_3 and Fe^0 were recorded for the nZVI exposed to the solution containing NO_3^- at 10 mM.

XPS analysis of nZVI extracted from the Cu or Zn solutions after 4 w indicated both Cu and Zn were present on the surface, i.e. sorbed only the nZVI (Fig. 6). Well defined Cu $2p_{1/2}$ and $2p_{3/2}$ satellite features at ~942 and ~963 indicated the presence of Cu^{2+} species. [20] The Cu $2p_{3/2}$ spectra was fitted with two peaks following the work of Biesinger et al. [21], which indicated the presence of Cu^0 (932.5 eV) and $Cu(OH)_2$ (934.2 eV). The detection of Cu^0 on the surface of nZVI is in agreement with previous work [19]. The Cu^{2+} ion was present because either it had been directly sorbed to the nZVI from solution (and not chemically reduced) and/or chemically reduced to Cu^0 and then reoxidised to Cu^{2+} (as $Cu(OH)_{2(s)}$). Due to the relatively close distance between the binding energies of Zn^0 and ZnO species (e.g. ~1021.65 and ~1021.0 eV respectively) mixed systems are difficult to quantify

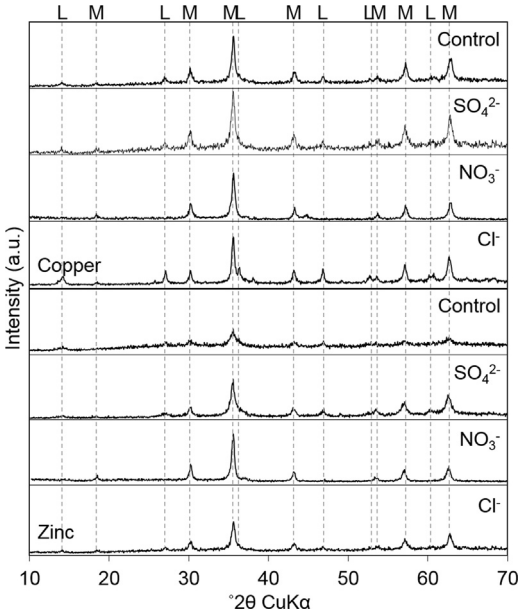

Fig. 5. X-ray diffraction plots with identified peaks for the range 10–70°2θ acquired for nZVI extracted from experimental solutions containing Cu (left) and Zn (right) and 10 mM Cl^-, NO_3^-, SO_4^{2-} and control after 4 w (ascending).
Key: L – γ-FeOOH and M – Fe_3O_4/γ-Fe_2O_3.

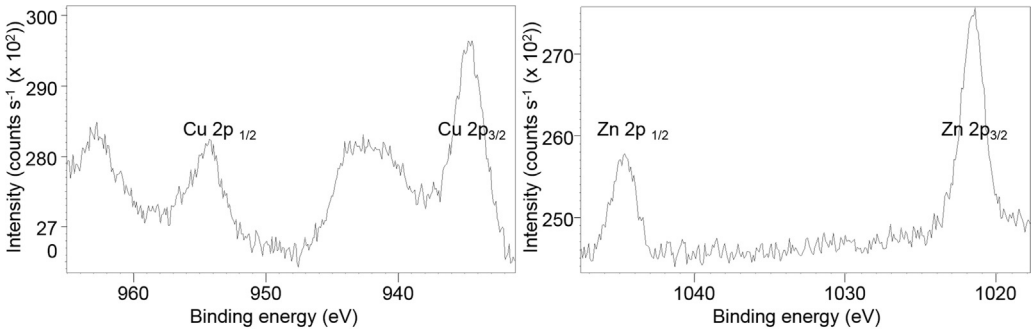

Fig. 6. Typical 2 p photoelectron spectra for nZVI removed from 0.3 mM Cu (left) and Zn (right) solutions after 4 w. Note, differing vertical scales.

due to spectral overlap, and therefore the specific Zn phase(s) present could not be determined using XPS.

4. Discussion

4.1. nZVI behaviour when exposed to chloride and sulphate containing solutions

The corrosion fate and reactivity (i.e. the ability to remove Cu and Zn) of nZVI when exposed to Cl^- and SO_4^{2-} containing solutions were broadly similar, and therefore these systems will be discussed together. After 16 w exposure, the degree of oxidation of nZVI exposed to 10 mM Cl^- and SO_4^{2-} was similar to the nZVI when exposed to the control solution (Fig. S6, Supplementary material). In general this agrees with previous work using hydrogen-reduced nZVI [9], although in such work the nZVI was exposed to a 10 mM SO_4^{2-} solution which resulted in a mixture of corrosion products: schwertmannite ($Fe_{16}O_{16}(OH)_y(SO_4)_z \cdot nH_2O$) and Fe_3O_4 [17]. The emergence of α-FeOOH (described as an end-product of an iron corrosion series) [17] in the 16 w XRD data was to considered to be the ultimate corrosion phase of nZVI in the current work.

At high concentrations, Cl^- and SO_4^{2-} increased both Cu and Zn remobilisation above control levels. Both Cl^- and SO_4^{2-} are regarded as inert with respect to reduction by nZVI (i.e. not redox amenable) [5]. However, these anions have been observed to increase the corrosion rate of Fe^0 by raising the iron oxide layer dissolution rate [2,4,5], with the breakdown of this layer leading to a localised corrosion of the underlying metal. Pitting corrosion, an electrochemical oxidation-reduction process, has been observed to occur on the surface of metals coated with a passive film with both Cl^- [22] and SO_4^{2-} anions [23]. This process leads to a decrease in solution pH due to hydrolysis [24], which in turn causes an acceleration of the corrosion process. This was observed for the 10 mM Cl^- and SO_4^{2-} solutions where increased dissolved iron concentrations (Fig. 4) and low pH levels (Figs. S4 and S5, Supplementary material) were recorded. The greater remobilisation of Cu and Zn into solution from the surface of nZVI was attributed to this pitting corrosion process, with the breakdown of the passive iron surface (the adsorption sites). Being a non-reduced surface complex, Zn is more sensitive to such disturbances at the iron surface, which was shown in the increased remobilisation when compared to Cu.

4.2. Bicarbonate

Bicarbonate is not considered to be reducible by Fe^0. However, the anion's role in corrosion is not simple, as both precipitation of $FeCO_3$ can result in passivation of the nZVI surface [25,26], and adsorbed H_2CO_3 and HCO_3^- can react as oxidants providing cathodic reactions that drive nZVI corrosion. In this work, it was evident that HCO_3^- caused an acceleration in the nZVI corrosion when compared to the control (Fig. S3, Supplementary material), which has been observed in a previous study with hydrogen-reduced nZVI [9]. This was evidenced by the emergence of the corrosion 'end-product' α-FeOOH, and the predominance of this phase after 16 w exposure (Fig. 3). It is thought that an initial film of iron carbonate forms ($FeCO_3$) readily oxidises (by DO) to Fe_2O_3 [27,28], which explains why iron-carbonate compounds such as siderite, were not detected in any XRD scans; further oxidation of Fe_3O_4/γ-Fe_2O_3 will produce γ-FeOOH [29], but the formation of this phase has been observed to be suppressed or totally eliminated in solutions containing appreciable concentrations of HCO_3^- ions, with the formation of α-FeOOH typically occurring instead [30], which was observed in this study. It has been suggested that carbonate anions directly interact with the iron, polymerising the double bands of $FeO_3(OH)_3$ octahedra common to both γ-FeOOH and α-FeOOH minerals toward a corner sharing arrangement, and thereby to the latter phase [30].

4.3. Nitrate

Unlike the other anions tested herein, NO_3^- is a reducible anion (when in the presence of Fe^0), and is known to greatly impact the ageing behaviour of Fe^0 [31,32]. In this work, as well as other studies [33,34], NO_3^- was shown to transform nZVI into an oxide (Fe_3O_4/γ-Fe_2O_3) rather than a hydroxide compound (e.g. γ-FeOOH/α-FeOOH). Anions like NO_3^- are thought to exchange with surface (hydr)oxide ligands to coordinate with oxide–matrix metal ions [4], although there is little agreement on the precise physical and chemical characteristics of this layer; studies have reported highly disordered γ-Fe_2O_3 at the surface, with Fe_3O_4 beneath, again in a disordered state [35,36]. The formation of the γ-Fe_2O_3 layer has been proposed to occur via the direct reaction with Fe^0 or by the oxidation of pre-existing Fe_3O_4 (a common corrosion product of iron) by NO_3^-. The formation of this layer would account for the lack of remobilisation of metals in the NO_3^- solutions (Table 2). This process has been observed to be relatively rapid; the metastable iron phase schwertmannite, detected on hydrogen-reduced nZVI, did not transform to another mineral phase when exposed to a 10 mM NO_3^- solution before passivation occurred [9]. This suggests that passivation occurs after the adsorption of the metal contaminant, but before remobilisation can occur (<2 h, Table 2), therefore enmeshing the metals into the surface oxide layer. The low iron concentrations recorded for the NO_3^- solutions further confirmed this process (Table 2 and Fig. 4), and therefore ferrous species may not be involved in the Cu or Zn uptake process. Passivation of nZVI surfaces with NO_3^- has been reported to occur above concentrations of 3 and 5 mM [5,9]. This work suggests that these figures are too high, and passivation would occur at lower NO_3^- concentrations. Greater passivation was observed, however,

for the higher concentration NO_3^- solutions (Fig. S6, Supplementary material); Fe^0 was detected in the XRD data (44.9 °2θ) of nZVI removed from the 10 mM NO_3^--Cu solution. The presence of Fe^0 further implied that the formation of the passivating layer was rapid, because Fe^0 was generally not detected within the XRD data recorded for nZVI extracted from solutions containing Cu and HCO_3^-, Cl^- or SO_4^{2-} after 1 d of aqueous exposure time.

The minimum nitrate concentration of 0.1 mM (6.2 mg L^{-1}) which enabled long-term Cu and Zn retention on nZVI was considerably lower than the European Drinking Water Directive's maximum limit for NO_3^- in water (50 mg L^{-1}). However, NO_3^- is a widespread contaminant in groundwaters and surface waters [37] and as such care must be taken to ensure that if nZVI and NO_3^- were simultaneously injected into an aquifer for remediation purposes that the process does not result in NO_3^- groundwater contamination.

4.4. Cations

Results herein demonstrate that Cu cations were able to oxidise nZVI more rapidly than Zn cations. This can be related to the influence of galvanic coupling, i.e. sacrificial corrosion of nZVI upon formation of a galvanic cell with a redox amenable specie. This was likely to have occurred in solutions containing Cl^- and SO_4^{2-}, but not in solutions containing NO_3^- due to its aforementioned passivating influence.

The difference in Cu and Zn remobilisation times (Table 2) was ascribed to the differing uptake mechanism of each metal onto the nZVI. Cu was likely to have been chemically reduced [19] while Zn was likely to have been adsorbed onto the surface, followed by complexation [38]. This suggests that an oxidation step (by the presence of DO) was required for remobilisation of the former species. This was corroborated by both Cu^0 and Cu^{2+} species being detected at the surface of the nZVI (in the XPS data), whereas Zn was not; Zn can more easily desorb from the nZVI because it is not as redox amenable (not chemically reduced), and therefore may require a constant flow of electrons to remain complexed at the Fe surface.

5. Conclusions

For over a decade nZVI has received much attention as a new technology for contaminated land treatment. Despite such interest there still remains fundamental knowledge gaps with regard to the influence of common groundwater anions on both aqueous contaminant uptake onto nZVI and the environmental transformation and fate of nZVI. This study has attempted to bridge this gap by directly comparing the influence of HCO_3^-, Cl^-, SO_4^{2-} and NO_3^- on the aqueous corrosion of nZVI and associated removal efficacy of aqueous Cu and Zn. The following can be concluded:

i) The corrosion rate of nZVI was recorded to follow the order (from most reactive to most passive) of: $HCO_3^- > Cl^-/SO_4^{2-} >$ no anions $> NO_3^-$. When nZVI was exposed for 16 w to a 10 mM HCO_3^- solution the main corrosion product phase was α-FeOOH. In contrast, Fe_3O_4/γ-Fe_2O_3 was recorded as the main nZVI corrosion product phase for solutions containing Cl^- or SO_4^{2-}, with a minor contribution from γ-FeOOH and α-FeOOH. The main nZVI corrosion product phase when exposed to NO_3^- was Fe_3O_4/γ-Fe_2O_3.

ii) The ability of nZVI to initially remove Cu and Zn from solution was not influenced by common groundwater anions (near-total removal in all systems was recorded). However, the long-term retention of Cu and Zn by nZVI was strongly influenced by the presence of Cl^-, SO_4^{2-} and NO_3^-. This phenomena was recorded to only occur when anions were present at 10 mM concentrations, with Cu and Zn largely unaffected when the anions were present at concentrations below 1.0 mM. Cu and Zn desorption from the nZVI was recorded to be enhanced by the presence of both SO_4^{2-} and Cl^- at 10 mM. This was ascribed to pitting corrosion (driven by the presence of SO_4^{2-} and Cl^-) which acts to destabilise the iron surface and allow sorbed metals to be released back into solution. Very little desorption of Cu and Zn was recorded for solutions containing NO_3^- due to passivation of the nZVI surface.

Overall the results demonstrate that HCO_3^-, Cl^-, SO_4^{2-} and NO_3^- have considerable influence on both nZVI aqueous corrosion behaviour and heavy metal retention. Whilst Cl^- and SO_4^{2-} bearing solutions were recorded to enhance nZVI corrosion rate and also cause Cu and Zn desorption, the opposite was recorded for solutions containing NO_3^-. It is therefore suggested that nitrate could be utilised as a complimentary chemical to prevent metal desorption from nZVI and thus improve its long-term performance for in situ water treatment applications.

Acknowledgements

We would like to thank Mr Jonathan Jones (School of Chemistry) from the University of Bristol for performing TEM analysis. Furthermore, we would like to thank Dr Chung Choi (School of Earth Sciences) for the use and advice on ICP-OES analysis. This work was financially supported with funding from the National Environment Research Council (NERC).

Appendix A. Supplementary data

Supplementary data associated with this article can be found, in the online version, at http://dx.doi.org/10.1016/j.jece.2017.01.038.

References

[1] A. Henderson, A. Demond, Long-term performance of zero-valent iron permeable reactive barriers: a critical review, Environ. Eng. Sci. 24 (2007) 401–423, doi:http://dx.doi.org/10.1089/ees.2006.0071.
[2] J. Devlin, K. Allin, Major anion effects on the kinetics and reactivity of granular iron in glass-encased magnet batch reactor experiments, Environ. Sci. Technol. 39 (2005) 1868–1874, doi:http://dx.doi.org/10.1021/es040413q.
[3] M. Stuart, P. Chilton, D. Kinniburgh, D. Cooper, Screening for long-term trends in groundwater nitrate monitoring data, Q. J. Eng. Geol. Hydrogeol. 40 (2007) 361–376, doi:http://dx.doi.org/10.1144/1470-9236/07-040.
[4] T. Johnson, W. Fish, Y. Gorby, P. Tratnyek, Degradation of carbon tetrachloride by iron metal: complexation effects on the oxide surface, J. Contam. Hydrol. 29 (1998) 379–398, doi:http://dx.doi.org/10.1016/S0169-7722(97)00063-6.
[5] Y. Liu, T. Phenrat, G. Lowry, Effect of TCE concentration and dissolved groundwater solutes on NZVI-promoted TCE dechlorination and H2 evolution, Environ. Sci. Technol. 41 (2007) 7881–7887, doi:http://dx.doi.org/10.1021/es0711967.
[6] P. Keith, C. Lai, P. Kjeldsen, I. Lo, Effect of groundwater inorganics on the reductive dechlorination of TCE by zero-valent iron, Water Air Soil Pollut. 162 (2005) 401–420, doi:http://dx.doi.org/10.1007/s11270-005-7420-7.
[7] O. Schlicker, M. Ebert, M. Fruth, M. Weidner, W. Wust, A. Dahmke, Degradation of TCE with iron: the role of competing chromate and nitrate reduction, Ground Water 38 (2000) 403–409, doi:http://dx.doi.org/10.1111/j.1745-6584.2000.tb00226.x.
[8] J. Klausen, J. Ranke, R. Schwarzenbach, Influence of solution composition and column aging on the reduction of nitroaromatic compounds by zero-valent iron, Chemosphere 44 (2001) 511–517, doi:http://dx.doi.org/10.1016/S0045-6535(00)00385-4.
[9] B. Reinsch, B. Forsberg, L. Penn, C. Kim, G. Lowry, Chemical transformations during aging of zerovalent iron nanoparticles in the presence of common groundwater dissolved constituents, Environ. Sci. Technol. 44 (2010) 3455–3461, doi:http://dx.doi.org/10.1021/es902924h.
[10] S. Kanel, B. Manning, L. Charlet, H. Choi, Removal of arsenic(III) from groundwater by nanoscale zero-valent iron, Environ. Sci. Technol. 39 (2005) 1291–1298 http://www.ncbi.nlm.nih.gov/pubmed/15787369 (Accessed 21 October 2016).
[11] T. Lim, B. Zhu, Effects of anions on the kinetics and reactivity of nanoscale Pd/Fe in trichlorobenzene dechlorination, Chemosphere 73 (2008) 1471–1477, doi:http://dx.doi.org/10.1016/j.chemosphere.2008.07.050.

[12] R. Crane, H. Pullin, J. Macfarlane, M. Silion, I. Popescu, M. Andersen, et al., Field application of iron and iron-nickel nanoparticles for the ex situ remediation of a uranium-bearing mine water effluent, J. Environ. Eng. 141 (2015) 1–12, doi:http://dx.doi.org/10.1061/(asce)ee.1943-7870.0000936.
[13] G. Glavee, K. Klabunde, C. Sorensen, G. Hadjipanayis, Chemistry of borohybride reduction of iron(II) and iron(III) ions in aqueous and nonaqueous media. Formation of nanoscale Fe, FeB, and Fe2B powders, Inorg. Chem. 34 (1995) 28–35.
[14] A. Grosvenor, B. Kobe, M. Biesinger, N. McIntyre, Investigation of multiplet splitting of Fe 2p XPS spectra and bonding in iron compounds, Surf. Interface Anal. 36 (2004) 1564–1574, doi:http://dx.doi.org/10.1002/sia.1984.
[15] J. Nurmi, P. Tratnyek, V. Sarathy, D. Baer, J. Amonette, K. Pecher, et al., Characterization and properties of metallic iron nanoparticles: spectroscopy, electrochemistry, and kinetics, Environ. Sci. Technol. 39 (2004) 1221–1230.
[16] H. Pullin, R. Springell, S. Parry, T. Scott, The effect of aqueous corrosion on the structure and reactivity of zero-valent iron nanoparticles, Chem. Eng. J. 308 (2017) 568–577, doi:http://dx.doi.org/10.1016/j.cej.2016.09.088.
[17] R. Cornell, U. Schwertmann, The Iron Oxides: Structure, Properties, Reactions, Occurrences and Uses, John Wiley & Sons, Weinheim, FRG, 2003, doi:http://dx.doi.org/10.1002/3527602097.
[18] L. Signorini, L. Pasquini, L. Savini, R. Carboni, F. Boscherini, E. Bonetti, et al., Size-dependent oxidation in iron/iron oxide core-shell nanoparticles, Phys. Rev. B. 68 (2003) 1–8, doi:http://dx.doi.org/10.1103/PhysRevB.68.195423.
[19] X. Li, W. Zhang, Sequestration of metal cations with zerovalent iron nanoparticles: a study with high resolution X-ray photoelectron spectroscopy (HR-XPS), J. Phys. Chem. C 111 (2007) 6939–6946, doi:http://dx.doi.org/10.1021/jp0702189.
[20] M. Farquhar, J. Charnock, K. England, D. Vaughan, Adsorption of Cu(II) on the (0001) plane of mica: a REFLEXAFS and XPS study, J. Colloid Interface Sci. 177 (1996) 561–567, doi:http://dx.doi.org/10.1006/jcis.1996.0070.
[21] M. Biesinger, L. Lau, A. Gerson, R. Smart, Resolving surface chemical states in XPS analysis of first row transition metals, oxides and hydroxides: Sc, Ti, V, Cu and Zn, Appl. Surf. Sci. 257 (2010) 887–898, doi:http://dx.doi.org/10.1016/j.apsusc.2010.07.086.
[22] M. Moreno, W. Morris, M. Alvarez, G. Duffó, Corrosion of reinforcing steel in simulated concrete pore solutions effect of carbonation and chloride content, Corros. Sci. 46 (2004) 2681–2699, doi:http://dx.doi.org/10.1016/j.corsci.2004.03.013.
[23] Z. Szklarska-Smialowska, The Pitting Corrosion of Iron in Sodium Sulphate, Pergamon, 1978, doi:http://dx.doi.org/10.1016/s0010-938x(78)80079-1.
[24] S. Traubenberg, R. Foley, The influence of chloride and sulfate ions on the corrosion of iron in sulfuric acid, J. Electrochem. Soc. 118 (1971) 1066–1070, doi:http://dx.doi.org/10.1149/1.2408248.
[25] K. Henn, D. Waddill, Utilization of nanoscale zero-valent iron for source remediation—a case study, Remediat. J. 16 (2006) 57–77, doi:http://dx.doi.org/10.1002/rem.20081.
[26] A. Agrawal, W. Ferguson, B. Gardner, J. Christ, J. Bandstra, P. Tratnyek, Effects of carbonate species on the kinetics of dechlorination of 1,1,1-trichloroethane by zero-valent iron, Environ. Sci. Technol. 36 (2002) 4326–4333, doi:http://dx.doi.org/10.1021/es025562s.
[27] J. Heuer, J. Stubbins, An XPS characterization of FeCO3 films from CO2 corrosion, Corros. Sci. 41 (1999) 1231–1243, doi:http://dx.doi.org/10.1016/S0010-938X(98)00180-2.
[28] D. López, W. Schreiner, S. de Sánchez, S. Simison, The influence of carbon steel microstructure on corrosion layers: an XPS and SEM characterization, Appl. Surf. Sci. 207 (2003) 69–85, doi:http://dx.doi.org/10.1016/S0169-4332(02)01218-7.
[29] C. Su, R. Puls, T. Krug, M. Watling, S. O'Hara, J. Quinn, et al., Travel distance and transformation of injected emulsified zerovalent iron nanoparticles in the subsurface during two and half years, Water Res. 47 (2013) 4095–4106, doi:http://dx.doi.org/10.1016/j.watres.2012.12.042.
[30] L. Carlson, U. Schwertmann, The effect of CO2 and oxidation rate on the formation of goethite versus lepidocrocite from an Fe(II) system at pH 6 and 7, Clay Miner. 25 (1990) 65–71, doi:http://dx.doi.org/10.1180/claymin.1990.025.1.07.
[31] F. Cheng, R. Muftikian, Q. Fernando, N. Korte, Reduction of nitrate to ammonia by zero-valent iron, Chemosphere 35 (1997) 2689–2695, doi:http://dx.doi.org/10.1016/S0045-6535(97)00275-0.
[32] S. Choe, Y. Chang, K. Hwang, J. Khim, Kinetics of reductive denitrification by nanoscale zero-valent iron, Chemosphere 41 (2000) 1307–1311, doi:http://dx.doi.org/10.1016/S0045-6535(99)00506-8.
[33] K. Sohn, S. Kang, S. Ahn, M. Woo, S. Yang, Fe(0) nanoparticles for nitrate reduction: stability, reactivity, and transformation, Environ. Sci. Technol. 40 (2006) 5514–5519, doi:http://dx.doi.org/10.1021/es0525758.
[34] D. Mishra, J. Farrell, Understanding nitrate reactions with zerovalent iron using tafel analysis and electrochemical impedance spectroscopy, Environ. Sci. Technol. 39 (2005) 645–650, doi:http://dx.doi.org/10.1021/es049259y.
[35] A. Onyszko, C. Kapusta, J. Sieniawski, EXAFS study of iron nanoparticles with oxide shell, Arch. Mater. Sci. Eng. 28 (2007) 597–600.
[36] H. Kim, T. Kim, J. Ahn, K. Hwang, J. Park, T. Lim, et al., Aging characteristics and reactivity of two types of nanoscale zero-valent iron particles (FeBH and FeH2) in nitrate reduction, Chem. Eng. J. 197 (2012) 16–23, doi:http://dx.doi.org/10.1016/j.cej.2012.05.018.
[37] J. Nolan, K. Weber, Natural uranium contamination in major U.S. aquifers linked to nitrate, Environ. Sci. Technol. Lett. 2 (2015) 215–220, doi:http://dx.doi.org/10.1021/acs.estlett.5b00174.
[38] W. Yan, A. Herzing, C. Kiely, W. Zhang, Nanoscale zero-valent iron (nZVI): Aspects of the core-shell structure and reactions with inorganic species in water, J. Contam. Hydrol. 118 (2010) 96–104, doi:http://dx.doi.org/10.1016/j.jconhyd.2010.09.003.